Elsevier Editorial System(tm) for Ultrasonics
Manuscript Draft

Manuscript Number:

Title: Coded waveforms for optimised air-coupled ultrasonic nondestructive evaluation

Article Type: Special Issue: Memory of Bernard Hosten

Section/Category: SI: memory of Bernard Hosten

Keywords: ultrasonic, air-coupled, coded waveforms, cross-correlation, non-destructive evaluation

Corresponding Author: Dr Dave Hutchins,

Corresponding Author's Institution:

First Author: Dave Hutchins, PhD

Order of Authors: Dave Hutchins, PhD; Lee Davis, PhD; Marco Ricci, PhD; Stefano Laureti, MSc

Abstract: This paper investigates various types of coded waveforms that could be used for air-coupled ultrasound, using a pulse compression approach to signal processing. These are needed because of the low signal-to-noise ratios that are found in many air-coupled ultrasonic nondestructive evaluation measurements, due to the large acoustic mismatch between air and many solid materials. The various waveforms, including both swept-frequency signals and those with binary modulation, are described, and their performance in the presence of noise is compared. It is shown that the optimum choice of modulation signal depends on the bandwidth available and the type of measurement being made.

Coded waveforms for optimised air-coupled ultrasonic nondestructive evaluation

David Hutchins* and Lee Davis
School of Engineering, University of Warwick, Coventry CV4 7AL, UK

Marco Ricci and Stefano Laureti
Polo Scientifico Didattico di Terni, Università degli Studi di Perugia, 05100 Terni ITALY

Abstract—This paper investigates various types of coded waveforms that could be used for air-coupled ultrasound, using a pulse compression approach to signal processing. These are needed because of the low signal-to-noise ratios that are found in many air-coupled ultrasonic nondestructive evaluation measurements, due to the large acoustic mismatch between air and many solid materials. The various waveforms, including both swept-frequency signals and those with binary modulation, are described, and their performance in the presence of noise is compared. It is shown that the optimum choice of modulation signal depends on the bandwidth available and the type of measurement being made.

Keywords—ultrasonic, air-coupled, coded waveforms, cross-correlation, non-destructive evaluation

*Corresponding author: D.A.Hutchins@warwick.ac.uk

1. INTRODUCTION

Air-coupled ultrasound is a non-contact technique that is of interest to nondestructive evaluation (NDE), because it can be used to test a wide range of materials, from polymers and composites to metals [1,2], It can also be used in harsh environments, where contamination is an issue, and when rapid scanning is required. The technique has been proposed for application in many areas, including the inspection of composites [3-5], the detection of contamination and changes in food quality [6] and for imaging many other materials [7]. In all cases, it is the fact that air is used as the coupling medium which makes the technique unique.

In pioneering work by Bernard Hosten and his colleagues at CNRS Bordeaux, this approach has been used for the inspection of polymer composite plates using Lamb waves [8,9]. Work was also done on the determination of the elastic constants of carbon fibre reinforced polymer (CFRP) composites [10-12]. Here, the composite sample was positioned between an ultrasonic capacitive source/receiver pair, and the angle of incidence changed by rotation of the sample relative to the ultrasonic beam axis. The ultrasonic waveforms were recorded at each angle, and the longitudinal and shear wave arrival times calculated in real time (the latter created by mode conversion within the composite plate). Changes in arrival time were then compared to theoretical predictions, and an optimum fit of one with the other allowed the calculation of elastic constants. Elastic properties of other materials such as wood were also examined [13]. The design of the electrostatic (also known as capacitive) device is also important in determining performance [14].

Although air-coupled transducers can be scanned to form images, a higher resolution can be obtained if the transducer beam is focused. A convenient way to do this is to use external optics. This can be achieved using a Fresnel zone plate, which is aligned so as to focus on-axis at a pre-selected frequency [15]. More commonly, however, a good focus in air can be obtained across a wide bandwidth using external off-axis parabolic mirrors, which can be used for imaging thin materials and other samples [16,17]. They can also be used for point source experiments at solid surfaces with Lamb waves [18].

There is, however, a problem which must be overcome if air is used to transmit ultrasonic energy into and out of a solid sample – there is a need to overcome the large acoustic impedance mismatch between air and the solid object being tested. This causes several problems. The first is that a large fraction of the incident energy is reflected at the air/solid interface. This reduces the amount of energy both entering and leaving the sample. It also means that a large reflection from the incident surface results, meaning that pulse-echo

operation becomes more complicated. In through-transmission, there are two basic approaches to solving the lack of signal. The first is to choose a very narrow bandwidth, by use of a highly resonant, high amplitude source and receiver. The frequency of operation is then tuned to the through-thickness resonance of the sample, so as to maximize transmission [19]. This lack of bandwidth is a problem when it comes to conventional imaging, as discrimination of defects, for example, becomes very difficult.

The second approach is to use a wider bandwidth, together with some method of retrieving very small ultrasonic signals that have passed through two separate air/sample boundaries. This second method has been investigated by several authors [20,21], and the general approach is to use a form of cross-correlation to detect the signal. The resulting technique is known as pulse compression. The incident waveform, with a bandwidth usually defined by the transduction method used, is chosen so that this type of signal processing can be performed most effectively for a particular measurement. There are many types of signal that can be used, but they can be broadly classified within two main types: a swept-frequency "chirp" signal or a form of binary sequence. Fig. 1 gives an example of a chirp signal buried in noise to illustrate the pulse compression process. Cross-correlation between the output "noisy" signal with a reference waveform, known in literature as matched filter, allows this signal to be detected, with the smoothed rectified output shown. The resulting pulse compression operation has allowed the signal to be enhanced in signal to noise ratio (SNR) properties, allowing air-coupled measurements to be made. Usually the matched filter coincides with a replica of the sent signal. Moreover, depending on the specific application, the pulse compression procedure can use either periodic or aperiodic signals, and as a consequence the cross-correlation step is then realized in a cyclic or non-cyclic mode respectively.

Fig. 1. (a) Example of a linear chirp signal embedded in noise, and (b) the resultant pulse compression output from a cross-correlation.

The operation shown in Fig. 1 is an example of a pulse compression operation that is not optimized. The purpose of this paper is to investigate some different forms of signal

modulation, and to determine the best approach for air-coupled ultrasound for a given bandwidth of measurement.

2. THE CHOICE OF WAVEFORM FOR PULSE COMPRESSION

Various forms of both chirp signals and binary sequences have been investigated in this research. Consider first chirp signals. Here, the frequency can be swept in either a linear or a non-linear way with respect to time. Two such signals sweeping from 100 kHz to 400 kHz are shown in Fig. 2. While at first sight the waveforms do not appear to be very different, their spectra indicate that the two signals have very different properties. This can be illustrated further by looking at the trajectory followed by the instantaneous frequency in the Time-Frequency plane, as shown in Fig. 3. In particular, the linear chirp is associated with a straight line in this type of plot, whereas the trajectory of the non-linear chirp can be any continuous monotonic curve, defined by the type of sweep function used.

Fig. 2.Examples of chirp signals in the form of (a) linear and (b) non-linear frequency sweeps. Waveforms are on the left, and corresponding frequency spectra are on the right.

Fig. 3.Trajectories in the Time-Frequency planes of linear and non-linear chirps

In addition, it is usual to apply different types of widows to linear chirps. This reduces the level of side-bands within the frequency spectrum, at the cost of a lower energy. There are many different types of window that can be used, but this work has investigated three types: Gaussian, Blackman and Tukey [22-23]. All three have different properties, depending on the type of information that is required.

The level of side-bands is determined by the cross-correlation of the input signal with the matched filter applied to the output signal. According to the Wiener–Khinchin theorem, the cross-correlation function is equal to the Inverse Fourier Transform of the Cross-Spectral Density of the input signal with the matched filter. Since in most cases the matched filter coincides with a shifted replica of the signal itself, the side-bands are determined by the Inverse Fourier Transform of the Power Spectral Density (PSD) of the input signal. It is well known that PSDs with abrupt changes give rise to slow attenuating side-bands: by applying a window function to a linear Chirp a smoothing of the PSD is obtained, thereby producing a faster decay of side-bands. At the same time, the effective bandwidth of the signal is reduced, causing a broadening of the main lobe of the cross-correlation, i.e. a worsening of the resolution. A trade-off exists between side-band reduction and resolution achievable by applying a windowing function and the three types here employed correspond to different points of the trade-off boundary.

With respect to non-linear chirps, windowing should be applied with caution, since the linear relationship between instantaneous frequency and time is no longer valid. However, the reduction of side-band levels is still of the utmost importance for obtaining a good result experimentally.

Thus, to tackle this problem, the possibility of performing windowing in the frequency domain (i.e. spectral windowing) on a non-linear chirp signal has been investigated. This can be achieved without relinquishing the constant envelope feature in the time-domain waveform. In addition, the same transmitted energy as that of a non-windowed linear chirp is maintained, while reducing side-band levels. As proposed in [24], this technique can be used for both linear chirps, and for various non-linear chirp signal types (such as Gaussian, Blackman and Tukey). This is achieved by starting from the PSDs of linear chirps, which are then windowed by the corresponding function.

Figure 4 illustrates the effect of time and spectral windowing when applied to chirp signals. It can be seen that time windowing of a linear chirp signal (on the left) provides very efficient reduction in side-band levels, and exhibits a distinct central lobe. On the other hand, spectral windowing of a non-liner chirp (to the right of the figure) ensures a resolution that is almost the same as for the un-windowed linear chirp. It provides a significant reduction of the side-band levels in the region close to the zero time point, while in the regions further away in time the side-band levels are almost the same as for the un-windowed chirp.

Fig. 4 *Comparison of the autocorrelation functions of chirp signals using both time windowing on a linear chirp (left) and spectral windowing on a non-linear chirp (right). In both*

cases, the un-widowed signal is shown in black and the Gaussian-windowed chirp is shown in grey.

Binary sequences can also take various forms. Golay sequences have been used in the past for ultrasonic measurements [25-26], and they exhibit the optimal auto-correlation characteristics both in the cyclic and non-cyclic case. However, they have to be used in pairs, and this aspect can be a limitation. This work has thus looked at other types of sequences. Three examples are shown in Figure 5. These all use a frequency of 300 kHz to represent a single bit within the sequences, but as can be seen, their appearance is very different, depending on the generation scheme used.

Fig.5. Examples of three types of binary sequence, (a) MLS, (B) Legendre Sequence, (c) Chaotic Sequence, that are useful for ultrasonic air-coupled signals, using a 300 kHz signal to represent one bit. The horizontal axis is the number of sample points in the waveform.

There are advantages to each of these types of binary sequence. If AC systems are considered, MLS and Legendre sequences allow the reconstruction of the impulse response without bias, and they are also more effective from a computational point of view than Golay sequences [27-29]. In particular, a fast transform exists for the MLS case, the Fast-M-transform, and this can outperform the standard correlation calculation via an FFT [30]. This could be important in real-time air-coupled imaging, for example. Note also that MLS and related sequences can be used in multi-input / multi-output systems by exploiting their pseudo-orthogonality [31]. Finally, MLS and Legendre sequences exhibit decimation properties (in particular the Legendre sequences are decimable for any integer) and this opens the possibility of sub-sampling the received signal efficiently in order to relax hardware constraints. The research has also looked at Chaotic sequences. These gained interest in communications systems, because of their flexible auto-correlation and cross-correlation properties [32].

In the following, these signals will be compared for use in air-coupled ultrasound. Their performance will be determined experimentally for various levels of noise, so that their suitability in NDT can be determined.

3. EXPERIMENTAL INVESTIGATION OF MODULATION SCHEME PERFORMANCE

The experiments were performed using a pair of capacitive transducers, aligned on-axis in air. These transducers have been described elsewhere [1,2], but can be used to generate and detect ultrasonic signals in air with a high efficiency. They use a thin metallised Mylar membrane attached to a micromachined backplate, and are designed to operate at frequencies of up to 1 MHz. Note that at frequencies higher than this, ultrasonic attenuation in air becomes very severe, limiting the range at which experiments can be performed for NDE purposes. The experimental impulse response of these devices is shown in Fig. 6. It can be seen that the experimental amplitude response for a pair of transducers peaks at approximately 300 kHz, and this is the reason for selecting this frequency for the binary sequences. The response also led to the choice of a frequency sweep range of 100 – 400 kHz for the chirp signals. The voltage drive signals were generated in LabView™ software, and sent to the transmitter via a National Instruments PXI system, as shown in Fig. 7. A DC bias was applied to the transmitter via a decoupling circuit. Signals were transmitted across the air gap, and detected by a capacitive transducer as an ultrasonic receiver. A charge amplifier was used to provide amplification and a DC bias to the receiver, before being recorded via the PXI system.

Fig. 6. Experimental ultrasonic transducer characteristics, showing (a) impulse response and (b) corresponding spectrum

Fig. 7 Schematic diagram of the apparatus for experiments in air

The first experiments recorded signals that were transmitted by each of a set of sequences across the air gap. This was done to determine the initial properties of the recorded signals in ideal conditions. The ultrasonic waveforms will not be the same as those provided by the

driving voltage sequences, due to the amplitude and phase response of the transducers, the effect of diffraction by the finite apertures of the transducers themselves, and frequency-dependent ultrasonic attenuation in air. It was thus important to determine the actual experimental response.

The experimental results can be illustrated by looking at two particular examples – a linear chirp and an MLS binary sequence. Fig. 8 illustrates the spectral content of these two types of signal used for the voltage drive waveforms. The chirp had a bandwidth defined by the chosen start and finish frequencies (100 - 400 kHz), whereas the MLS sequence had a spectrum resulting from the 300 kHz frequency used to define the repetition rate of a single bit. These signals were used to drive the ultrasonic air-coupled transmitter, and the signals detected by the receiver after propagation through air were recorded. The received experimental spectra in each case are shown in Fig. 9. Note that, as expected from Fig. 8, the MLS sequence exhibited the wider bandwidth. The received signal was now cross-correlated with the input, and the results obtained are shown in Fig. 9. It is clear from these results that the received MLS signal was not only an order of magnitude greater in amplitude, but that the width of the main cross-correlation peak was narrower.

Fig. 8. Spectral content of (a) chirp and (b) MLS signals used to drive the transducers in the experiments

Fig. 9. Received spectra derived from the ultrasonic waveforms of Fig. 7, for (a) chirp and (b) MLS signals

Fig.10. Cross-correlation outputs for experimental ultrasonic waveforms transmitted across air, for (a) chirp and (b) MLS signals. Also labeled are areas defined as the near and far regions of the outputs (see text).

The chirp and MLS signals were now examined for their performance in the presence of noise. The SNR was estimated by introducing artificial Additive White Gaussian Noise (AWGN) to the recorded data, before the cross-correlation/pulse compression procedure was implemented. The SNR was then measured in two ways: by increasing the noise in the near region (see Fig. 10), thereby investigating the influence of side lobes to the performance, and by increasing the noise in the far region to quantify the effect of noise on measurement resolution. The results are presented in Table 1. Here, the performance of MLS is compared in relative terms to those of the standard and cyclic forms of linear and nonlinear chirps. As previously indicated, in order to retrieve the impulse response of a system excited by a coded signal, two algorithms can be exploited: Cyclic and non-Cyclic Algorithm (henceforth called Standard). Cyclic algorithm exploits periodic excitation signal and process the steady-output signal in order to retrieve the impulse response by Cyclic Cross-Correlation. In the Standard Algorithm, the acquisition and cross-correlation is performed for a single shot of the excitation signal. As described further, Cyclic algorithm ensure a better SNR of the measurement than the Standard one, even if it introduces some constraints on the impulse response duration.

It is evident from Table 1 that all the signals achieved similar results, even though the non-linear chirp worked better than the others in the suppression of near side-lobes, while the standard linear chirp guarantee the best performances in the far side-lobe region. As an example, if the amplitude of input signals is 1V, for MLS you can still distinguish signal from noise in the near region at a value of 1/97 = 10.3 mV.

Table 1: Relative SNR levels in the near and far regions of the cross-correlation outputs

In order to explain the above results, consider first the binary sequences such as MLS. Here, for an acquisition time *T*, the theoretical Excitation Signal Energy (*E*) is given by

$$E = A^2 T \quad , \qquad (1)$$

noting that the duration of excitation is the same as that of the measurement. However, the noise energy (E_{noise}) is given by

$$E_{noise} = \sigma^2 T. \qquad (2)$$

In the case of chirp signals, two types can be considered: those with a cyclic and those with a standard acquisition algorithm. For the cyclic case, the duration of excitation is the same as that of the measurement (as for the MLS binary sequence). However, now the excitation signal energy is half that of the MLS sequence, whereas the noise energy is the same. In the standard chirp measurement scheme, the excitation is “on” for a time T, while the output signal is measured for a time $T + T_1$. The excitation signal energy is the same as for the cyclic case, but now the noise energy is higher, and is given by

$$E_{noise} = \sigma^2 (T+T_1) \qquad (3)$$

If the SNR values of the MLS sequence, the cyclic chirp and the standard chirp are SNR_{MLS}, SNR_{CYCLIC} and $SNR_{STANDARD}$ respectively, and if $T_1=T$, it follows that

$$SNR_{MLS} = A^2/\sigma^2; \qquad (4a)$$
$$SNR_{CYCLIC} = A^2/2\sigma^2; \qquad (4b)$$
$$SNR_{STANDARD} = A^2/4\sigma^2. \qquad (4c)$$

This means that binary sequences such as MLS have the maximum theoretical SNR. In order to fully exploit this higher input energy, both the amplifier and the transducers have to match the broad bandwidth nature of the MLS sequence used, otherwise the overall energy put into the system is reduced by exciting frequencies that are outside of the system band.

Table 1 shows that the actual SNR gain ensured by the pulse compression procedures is fairly similar for binary sequences and chirp signals, although chirp signals obtain higher values of SNR. Indeed the band-pass behavior of chirp signals counterbalances the higher energy carried by MLS sequences by fitting better to the overall transfer function of the experimental system, composed of the transducers and the amplifier. For the system considered here, which uses broad bandwidth air-coupled transducers, this effect ensures an extra factor of 2 in the SNR gain for the chirp signals with respect to MLS. This becomes even more important if the bandwidth of the system is reduced. In this case, only a small

portion of the input energy can be transferred to the measurement system if a standard MLS sequence is used. In contrast to this, the energy spectrum of a chirp signal can be tailored to the transducer bandwidth. Hence, the input energy in this case is always almost effectively delivered to the system, so that chirp signals are a good choice for transducers with a narrow bandwidth.

Note that often it is desirable to use binary signals experimentally, both for hardware reasons and for reduced computational costs. In addition, sub-modulation and spectrum design techniques can also be applied, in order to further improve the resulting SNR. By using such techniques, the binary sequences approach can be improved substantially.

4. THROUGH-TRANSMISSION ULTRASONIC EXPERIMENTS

Another important application of air-coupled ultrasonic systems is the NDE of solid samples. Many characteristics can be measured, such as time of flight, attenuation, and thickness/ velocity changes, as well as the presence of defects or other structural changes. The performance obtained will depend on the characteristics of the ultrasonic signal, and in particular, the chosen waveform and processing methods. In Table 1 above, the relative merits of the various approaches, based on MLs, linear and non-linear chirps, were compared, and the linear cyclic chirp found to perform the best in terms of SNR. In the following, their performance in actual air-coupled through-transmission experiments will be examined. Here, a sample was placed normal to the ultrasonic beam, as shown in Fig. 11 for a Plexiglas plate. This material has a longitudinal velocity of 2,700 ms^{-1}, and plates of thicknesses 0.1 mm, 1 mm and 5 mm were examined.

Fig. 11. Through-transmission experiments using a pair of capacitive ultrasonic transducers.

Figure 12 shows the cross-correlation outputs (equivalent to the impulse response of the whole measurement system) for the MLS signal and the three thicknesses of Plexiglas. The two responses are effectively similar for the two thinner samples. This is because their thickness is small enough that the frequency of the sample's fundamental resonance (at ~1.3 MHz for a 1mm thickness) is above that of the highest frequencies transmitted. At a thickness of 5 mm, however, where the solid plate through-thickness resonance would be expected at ~257 kHz, the impulse response is that of a decaying resonance. This is exactly what would be expected from such a system.

Fig. 12. Impulse response for the MLS sequence for three different thicknesses of Plexiglas: (a) 0.1 mm, (b) 1mm and (c) 5 mm.

Fig. 13 shows the equivalent response for the standard linear chirp signal. Note that now the impulse response for the 0.1 mm and 1 mm thick samples is of a different form to that for the MLS sequence, as expected. Note again that there is no evidence of a through-thickness resonance, simply a well-behaved time impulse with a very good SNR which is better than that from the MLS sequence (a trend in agreement with the results shown in Table 1). For a 5 mm thick plate, the response is closer to a step function, with a fast rise and a slower fall, the latter indicative of the form of the through-thickness resonance within the plate.

Fig. 13. Impulse response for the standard linear chirp signal for three different thicknesses of Plexiglas: (a) 0.1 mm, (b) 1mm and (c) 5 mm.

Finally, the results for the standard non-linear chirp are presented in Fig. 14. Note that the response is similar in form to that from the linear chirp, shown in Fig. 13. However, there is a less rapid rise in the initial response for the 5 mm thick sample, and a cleaner “tail” with evidence of the resonance seen in Fig. 12 (c) as a small modulation of the decaying amplitude.

Fig. 14. Impulse response for the standard non linear chirp signal for three different thicknesses of Plexiglas: (a) 0.1 mm, (b) 1mm and (c) 5 mm.

It is interesting to look at the frequency spectra corresponding to the impulse responses for the 5 mm thick Plexiglas sample, and these are shown in Fig. 15 for the three signals. All three have produced a good spectral response, indicating that the frequency of resonance could be estimated from the peak value. Both MLS and the linear chirp give thickness values of 5.2 mm, assuming a longitudinal velocity of 2,700 ms^{-1}, and the non-linear chirp estimates the value at 5.3 mm. However, the larger received amplitude of the impulse response for the MLS sequence (Fig. 12 (c)), and the narrower spectral response, shows that it represents the induced resonance more accurately, and is thus the preferred waveform for thickness measurements.

Fig. 15. Frequency spectra arising from the impulse responses for the 5 mm thick Plexiglas plate: (a) MLS, (b) linear chirp and (c) non-linear chirp. All vertical scales are arbitrary.

CONCLUSIONS

This paper has demonstrated that the types of signal used for air-coupled ultrasound must be chosen with care. The results have demonstrated that it is extremely important that the type of excitation signal used is chosen so as to match the bandwidth available in the experimental system. With respect to the enhancement of the SNR, MLS and Chirp signals achieve very similar results for wide bandwidth measurements. For a narrower available bandwidth, either a chirp signal should be used, or some form of spectral shaping must be

introduced into the MLS sequence. For Time-of-Flight measurement, the MLS has been seen to be the best choice. It gives the highest received amplitude, and the shortest impulse response when used in a through-transmission measurement. For defect detection purpose, where very low side-bands level are needed, linear and non-linear windowed chirps appear as the best solution.

ACKNOWLEDGEMENTS

MR and SL gratefully acknowledge Prof. Pietro Burrascano for his scientific support and PRIN 2009 project “Diagnostica non ditruttiva ad ultrasuoni tramite sequenze pseudo-ortogonali per imaging e classificazione automatic di prodotti industriali” for financial support.

REFERENCES

[1] Hutchins DA, Neild A, “Air-borne ultrasound transducers”, in Ultrasonic Transducers, K. Nakamura ed., Woodhead publishers (2012).
[2] Lionetto F, Tarzia A, Maffezzoli A. Air-coupled ultrasound: a novel technique for monitoring the curing of thermosetting matrices. IEEE Trans Ultrason Ferroelectr Freq Control. 54 (2007)1437.
[3] Castaings M, Cawley P, Farlow R, Hayward G, “Single Sided Inspection of Composite Materials Using Air Coupled Ultrasound”, Journal of Nondestructive Eval. 17 (998) 37.
[4] Kazys R, Demcenko A, Zukauskas E, Mazeika L. Air-coupled ultrasonic investigation of multi-layered composite materials. Ultrasonics. 44 Suppl. 1 (2006) 819.
[5] Masmoudi M, Castaings M. Three-dimensional hybrid model for predicting air-coupled generation of guided waves in composite material plates. Ultrasonics 52 (2012) 81.
[6] Pallav P, Hutchins DA, Gan TH. Air-coupled ultrasonic evaluation of food materials, Ultrasonics 49 (2009) 244.
[7] Delrue S, Van Den Abeele K, Blomme E, Deveugele J, Lust P, Matar OB. Two-dimensional simulation of the single-sided air-coupled ultrasonic pitch-catch technique for non-destructive testing. Ultrasonics 50 (2010) 188.
[8] Hosten B, Biateau C. Finite element simulation of the generation and detection by air-coupled transducers of guided waves in viscoelastic and anisotropic materials. Acoust Soc Am. 123 (2008) 1963.
[9] Castaings M, Hosten B. Lamb and SH waves generated and detected by air-coupled ultrasonic transducers in composite material plates. NDT&E International 34 (2001) 249.
[10] Hosten B, Hutchins DA, Schindel DW. Air-Coupled Ultrasonic Bulk Waves to Measure Elastic Constants in Composite Materials, Review of Progress in Quant. NDE, (1996) 1075.
[11] Hosten B, Hutchins DA, Schindel DW. Measurement of elastic constants in composite materials using air-coupled ultrasonic bulk waves. J. Acoust. Soc. Am. 99 (1996) 2116.
[12] Castaings M, Hosten B. Air-coupled measurement of plane wave, ultrasonic plate transmission for characterising anisotropic, viscoelastic materials. Ultrasonics 38 (2000) 781.
[13] Dahmen S, Ketata H, Ben Ghozlen MH, Hosten B. Elastic constants measurement of anisotropic Olivier wood plates using air-coupled transducers generated Lamb wave and ultrasonic bulk wave. Ultrasonics. 50 (2010) 502.
[14] L.Pizarro, D. Certon, M. Lethiecq, B. Hosten. Airborne Ultrasonic Electrostatic Transducers with Conductive Grooved Backplates: Tailoring their Center Frequency, Sensitivity and Bandwidth. Ultrasonics 37 (1999) 493.

[15] Schindel DW, Bashford AG, Hutchins DA. Chromatic aberration of an air-coupled ultrasonic Fresnel zone-plate". IEEE Trans. Ultras. Ferr. Freq. Contr. 46 (1999) 242.
[16] Hosten B, Castaings M. Parabolic mirror and air-coupled transducer for multimodal plate wave detection. Review of Progress in Quantitative Nondestructive Evaluation, edited by D. O. Thompson and D. E.Chimenti , AIP Press, New York, Vol. 22 (2002) 1243.
[17] Gan TH, Hutchins DA, Billson DR, Schindel DW. High resolution air-coupled imaging of thin materials. IEEE Trans. Ultras. Ferr. Freq. Contr. 50 (2003) 1516.
[18] Holland SD, Teles SV,. Chimenti DE. Air-coupled, focused ultrasonic dispersion spectrum reconstruction in plates. J. Acoust. Soc. Am. 115 (2004) 2866.
[19] Kelly SP, Farlow R, Hayward G. Applications of through-air ultrasound for rapid NDE scanning in the aerospace industry. IEEE Tran. Ultras. Ferr. Freq. Control. 43 (1996) 581.
[20] Gan TH, Hutchins DA, Green RJ, Andrews M, Harris PD., Non-contact high-resolution ultrasonic imaging of wood samples using coded chirp waveforms. IEEE Trans. Ultras. Ferr. Freq. Contr. 52 (2005) 280.
[21] Yanez Y, Garcia-Rodriguez M, Garcia-Hernandez MJ; J. Salazar, Turo A, Chavez JA. Lamb Wave Generation with an Air-Coupled Piezoelectric Array Using Different Square Chirp Modulation Schemes. Proc. 2007 IEEE Ultrasonics Symposium, 1844.
[22] Pallav P, Gan TH, Hutchins DA. Elliptical-Tukey chirp signal for high-resolution, air-coupled ultrasonic imaging. IEEE Trans. Ultras. Ferroelect. Freq. Contr. 54 (2007) 1530.
[23] Ricci M, Senni L, Burrascano P, Borgna R, Neri S, Calderini M. Pulse-compression ultrasonic technique for the inspection of forged steel with high attenuation. Insight 54 (2012) 91.
[24] Pollakowski M, Ermert H. Chirp signal matching and signal power optimization in pulse-echo mode ultrasonic nondestructive testing. IEEE Trans. Ultrason., Ferroelectr., Freq. Control. 41 (1994) 655.
[25] Golay MJE. Complementarv Series, IRE Trans. on Information Theory, IT-7 (1961) 82.
[26] Garcia-Rodriguez M, Yañez Y, Garcia-Hernandez MJ, Salazar J, Turo A, Chavez JA. Application of Golay codes to improve the dynamic range in ultrasonic Lamb waves air-coupled systems. NDT & E Intl. 43 (2010) 677.
[27] Golomb S. Shift Register Sequences. San Francisco, CA: Holden-Day, 1967.
[28] Schroeder M R. Integrated-impulse method measuring sound decay without using impulses. J. Acoust. Soc. Amer. 66 (1979) 497.
[29] Ricci M, Senni L, Burrascano P. Exploiting Pseudorandom Sequences to Enhance Noise Immunity for Air-Coupled Ultrasonic Nondestructive Testing. IEEE Trans. Instr. Meas. 61 (2012) 11.
[30] Cohn M, Lempel A. On fast M-sequence transforms. IEEE Trans. Inf. Theory IT-23 (1977) 135.
[31] Sarwate D V, Pursley M B. Cross-correlation properties of pseudo-random and related sequences. Proc. IEEE, 68 (1980) 593.
[32] Setti G, Mazzini G, Rovatti R, Callegari S. Statistical Modeling of Discrete-Time Chaotic Processes—Basic Finite-Dimensional Tools and Applications. Proc. of the IEEE 90 (2002) 662.

Figure 1

Click here to download high resolution image

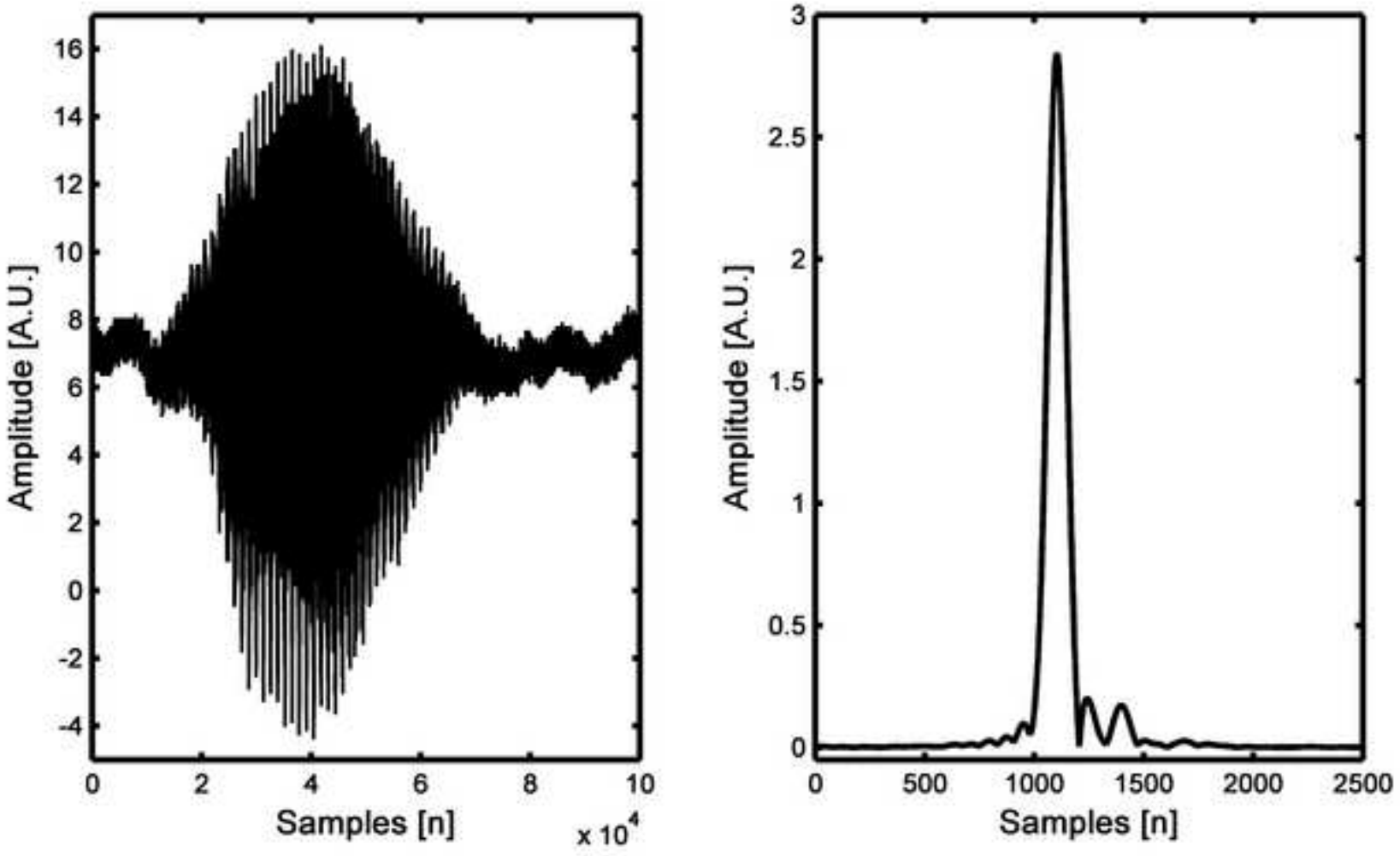

Figure 2

Click here to download high resolution image

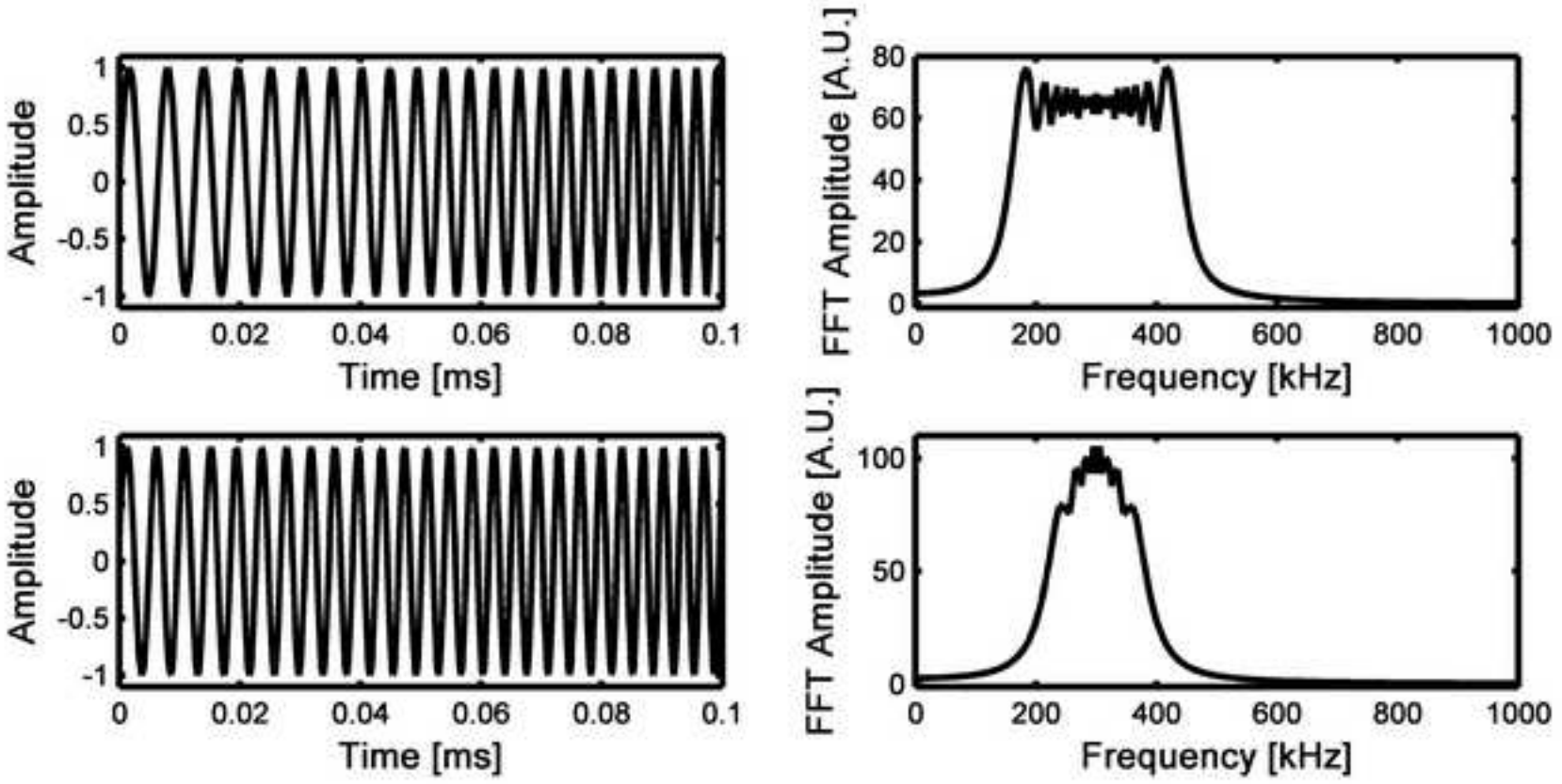

Figure 3

Click here to download high resolution image

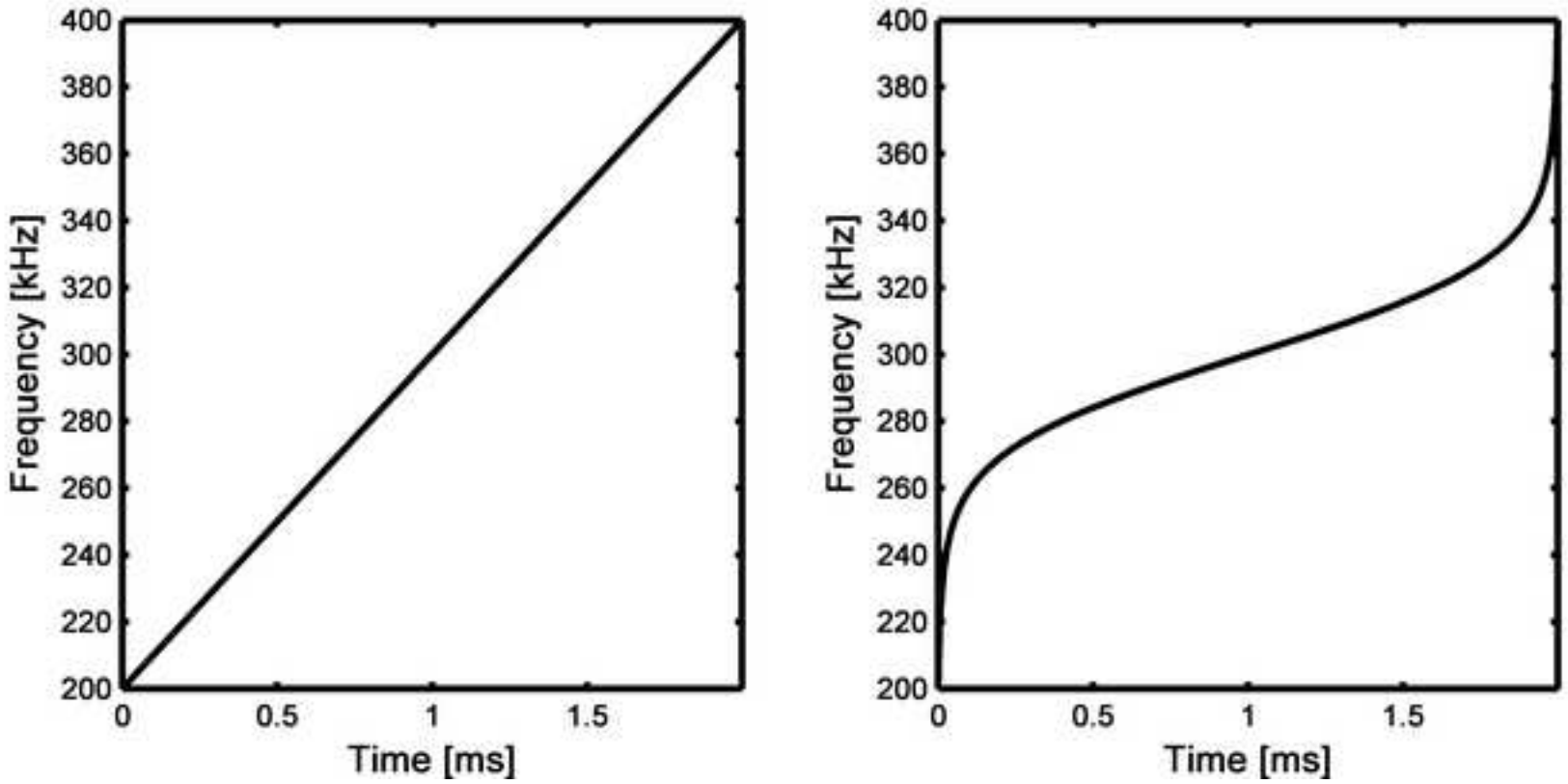

Figure 4

Click here to download high resolution image

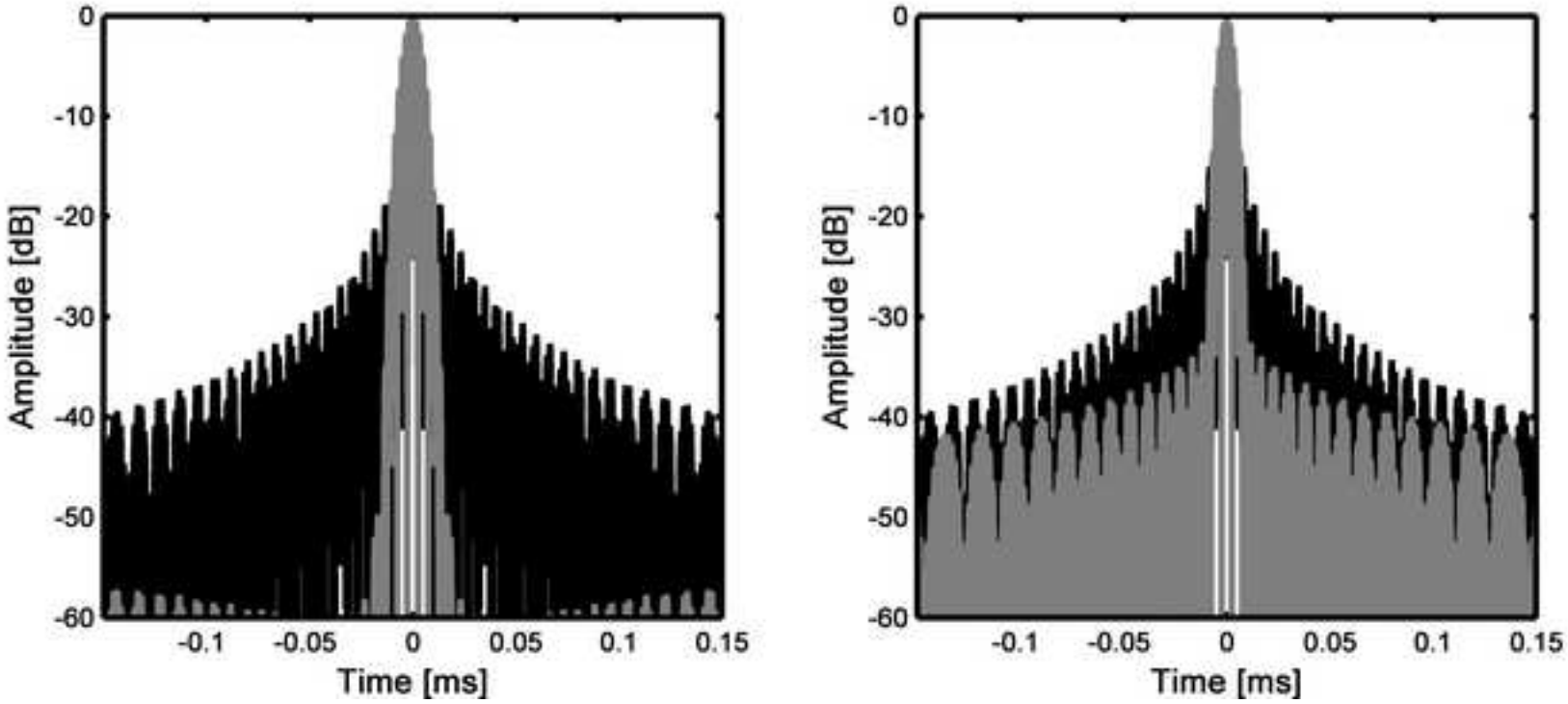

Figure 5

Click here to download high resolution image

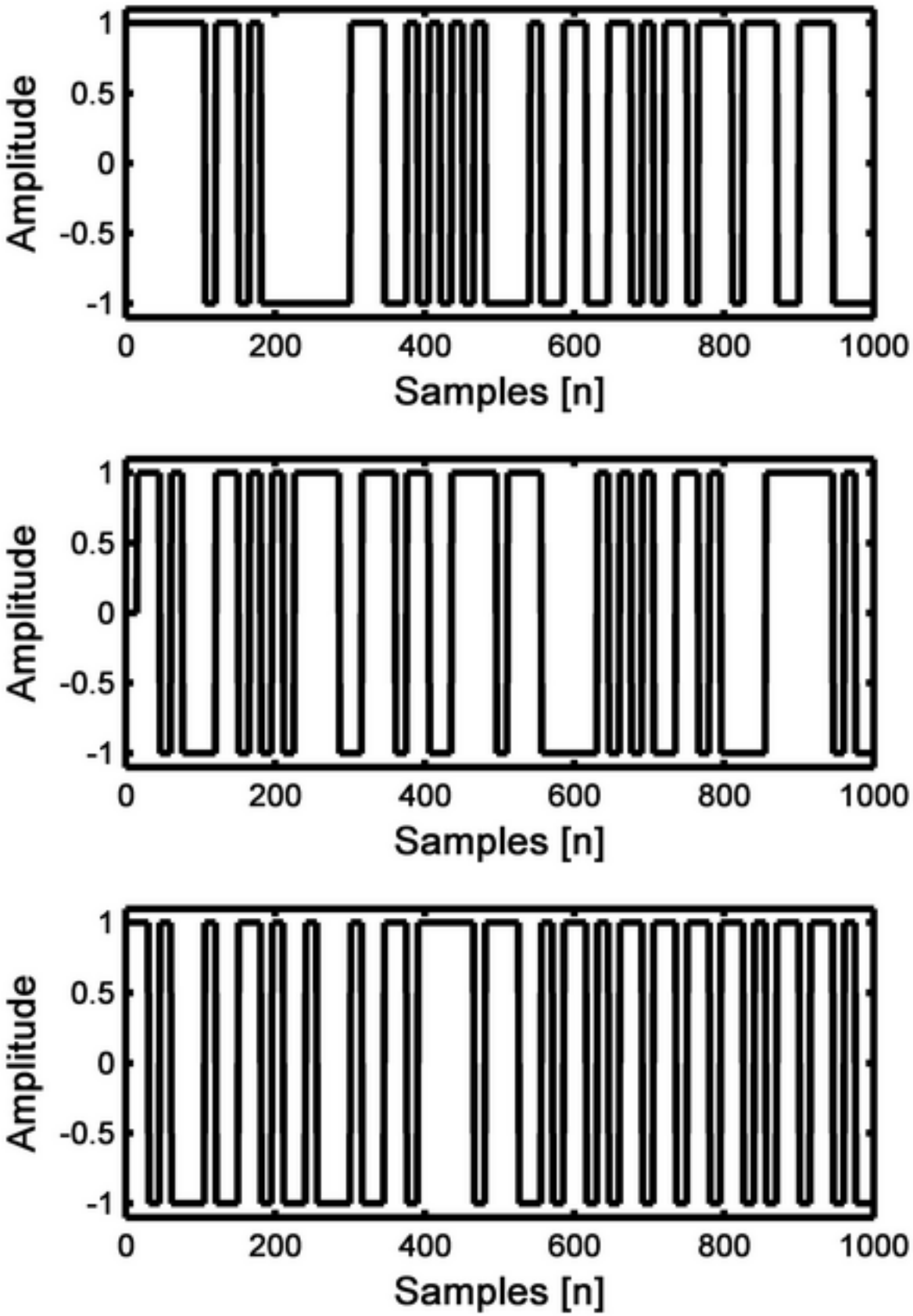

Figure 6

Click here to download high resolution image

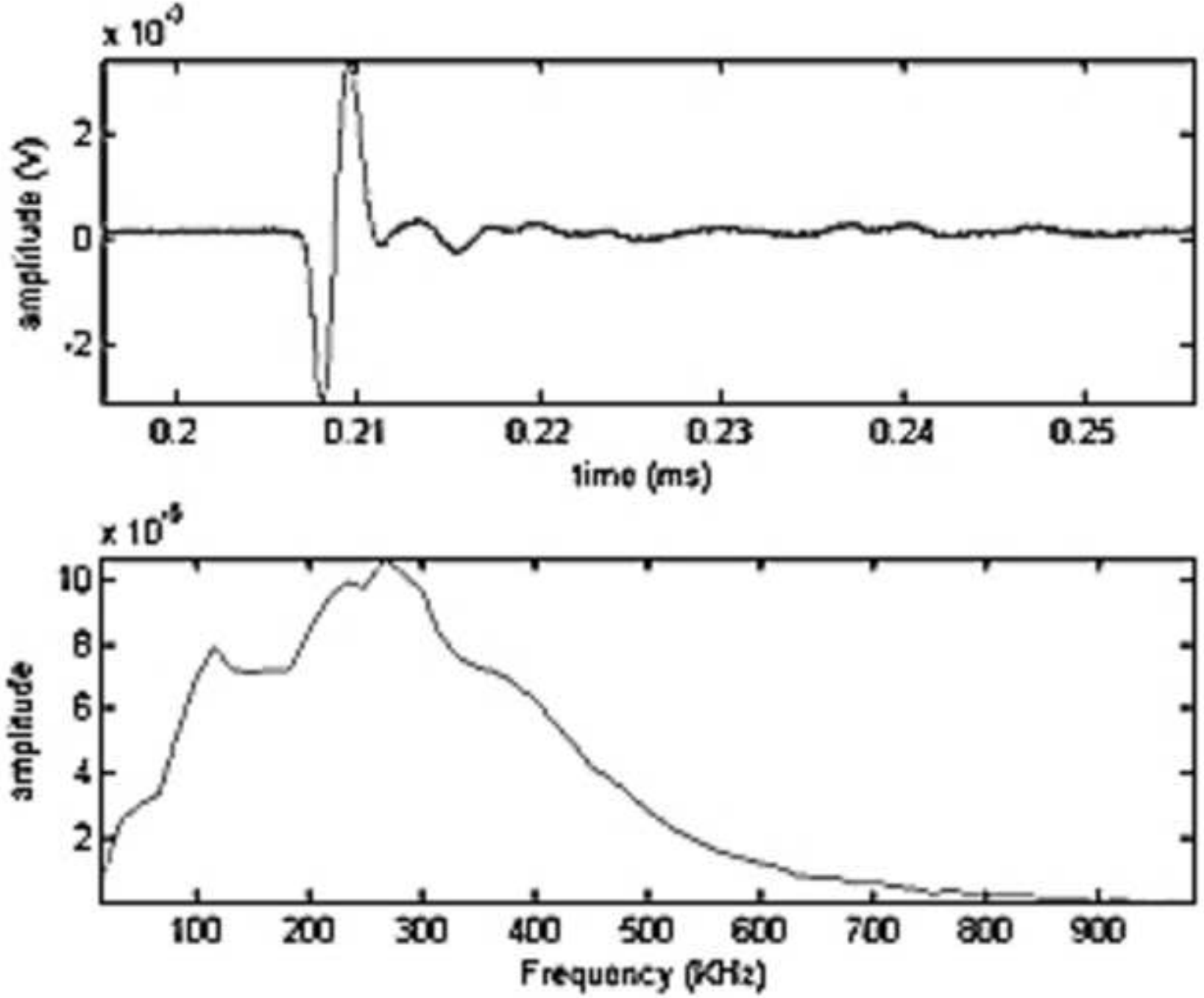

Figure 7

Click here to download high resolution image

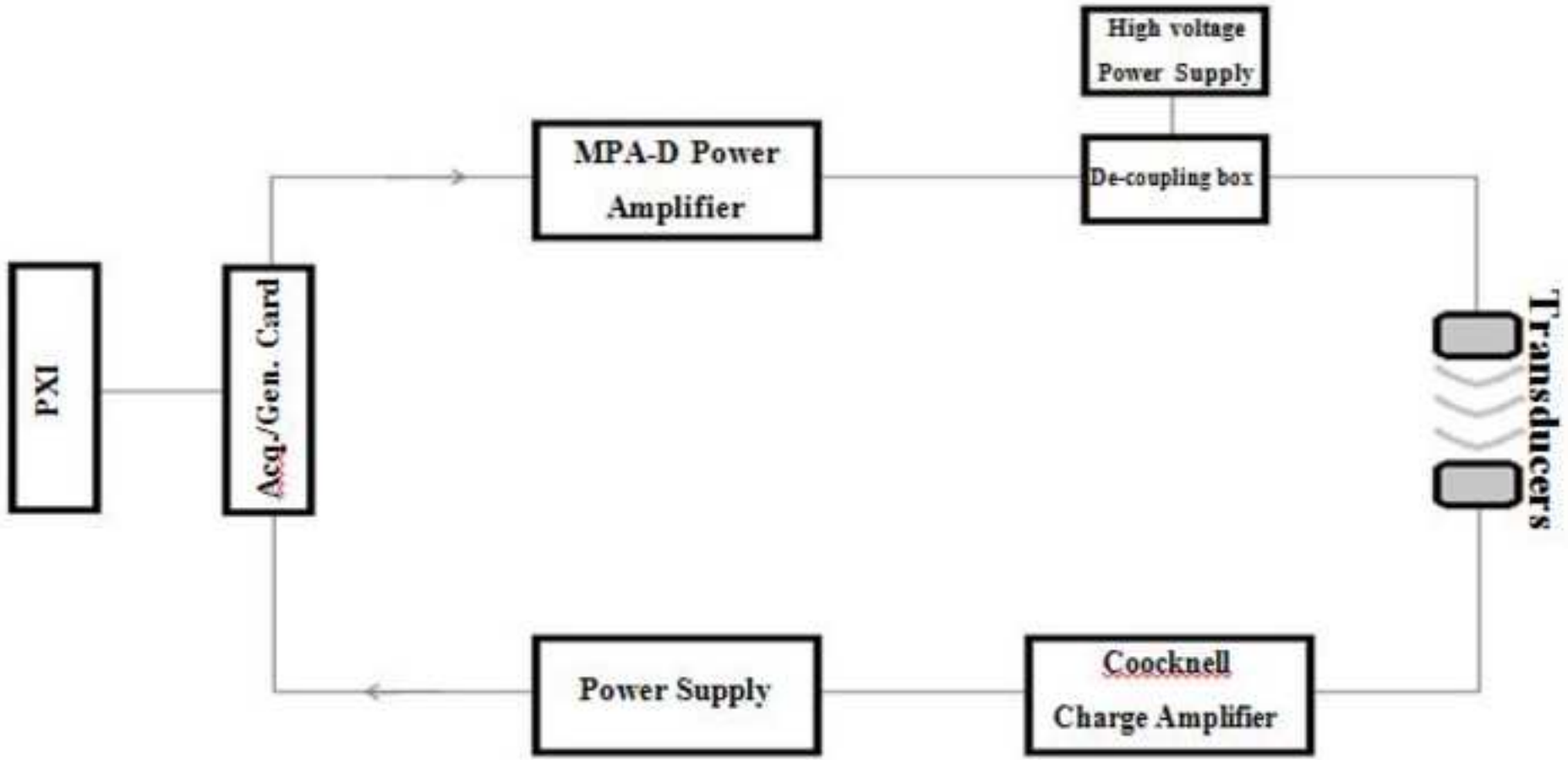

Figure 8

Click here to download high resolution image

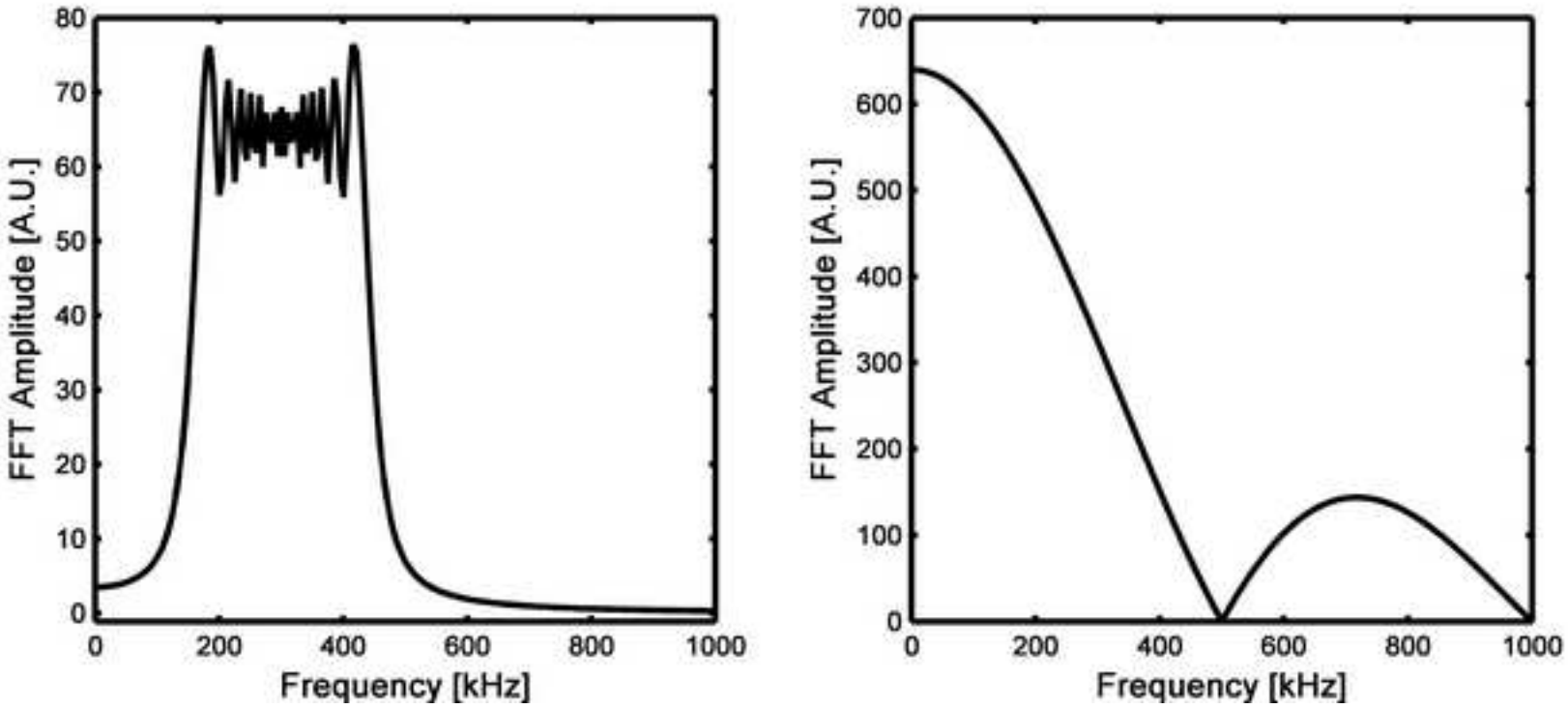

Figure 9

Click here to download high resolution image

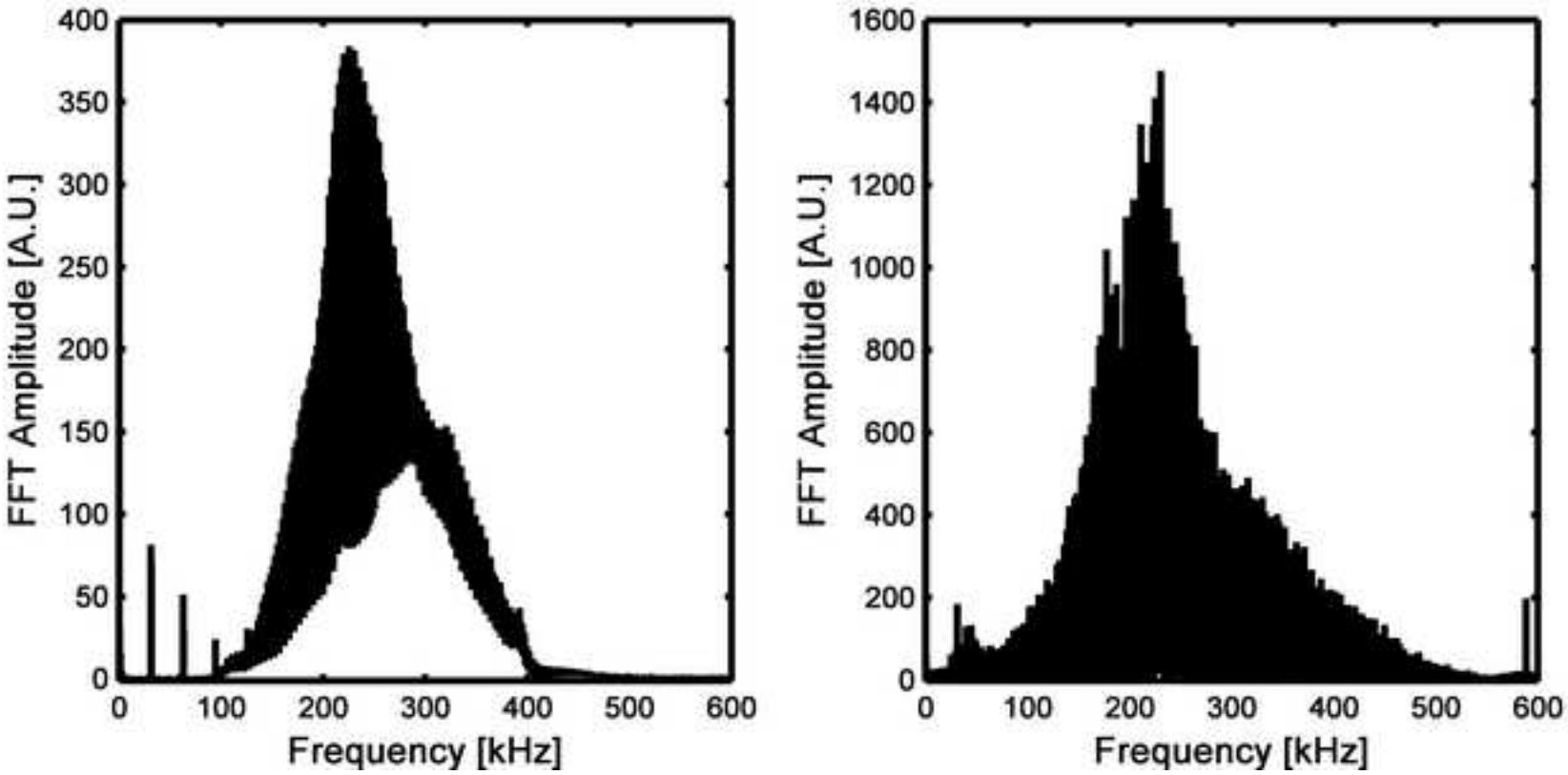

Figure 10

Click here to download high resolution image

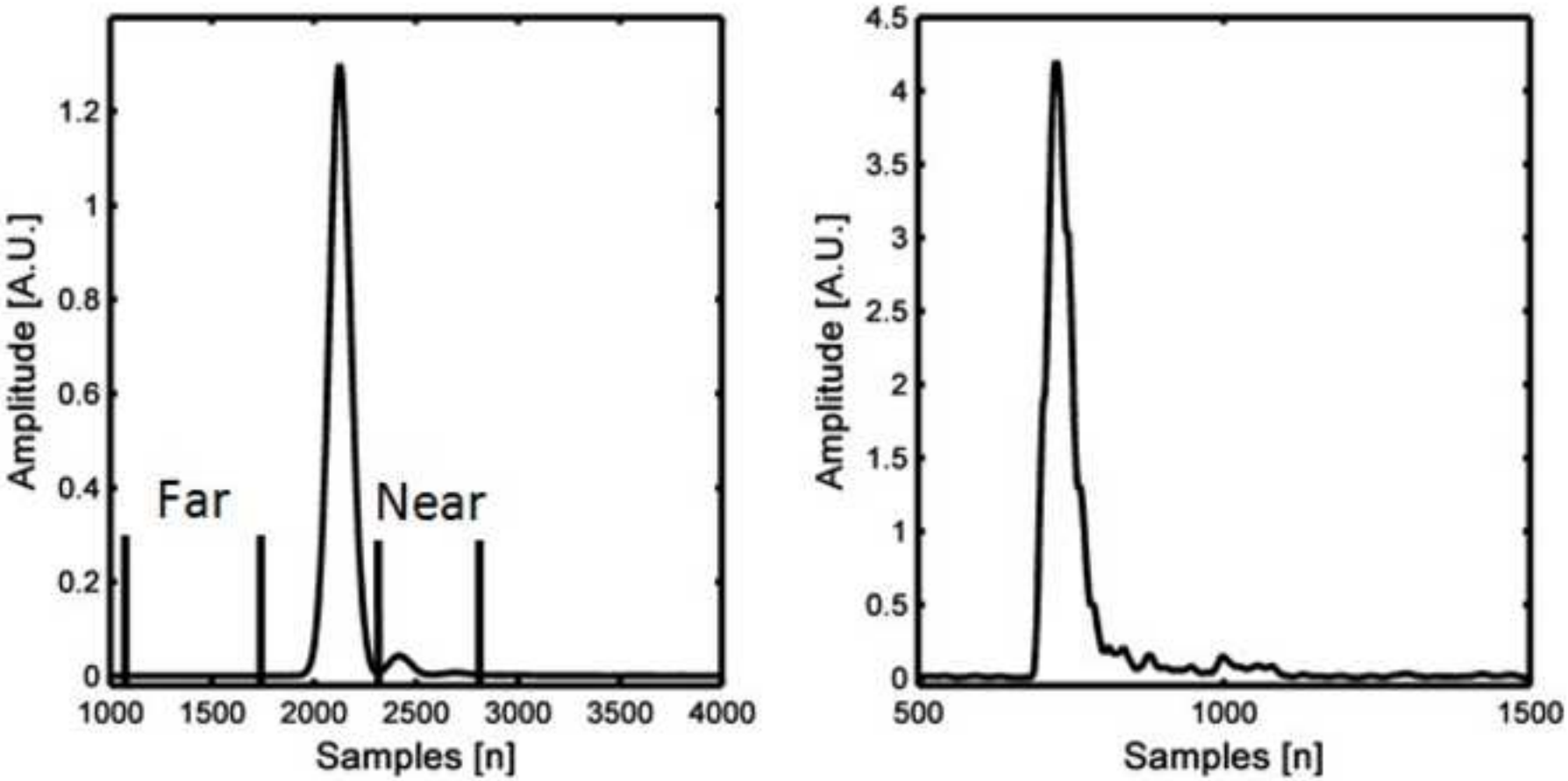

Figure 11

Click here to download high resolution image

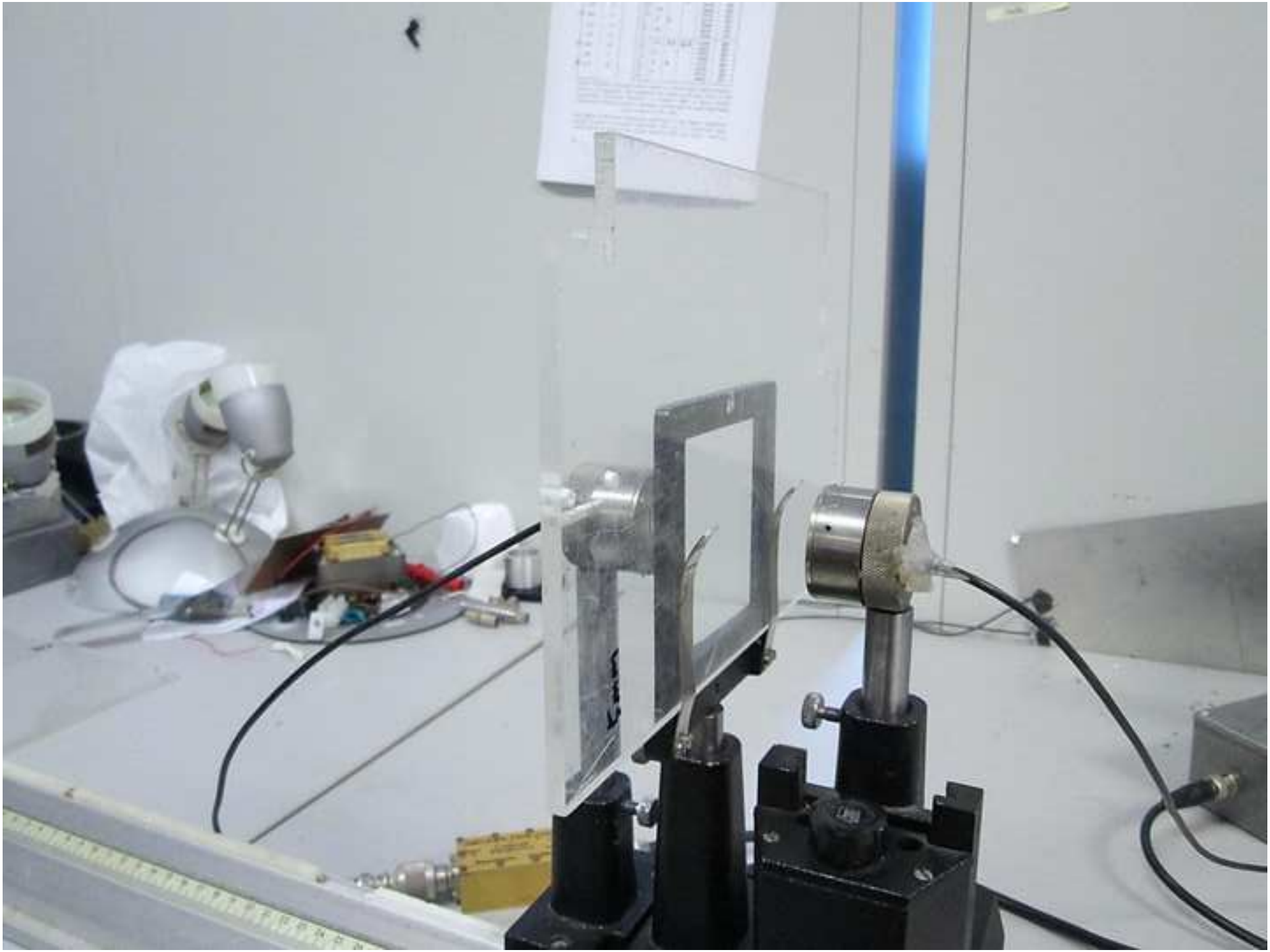

Figure 12
Click here to download high resolution image

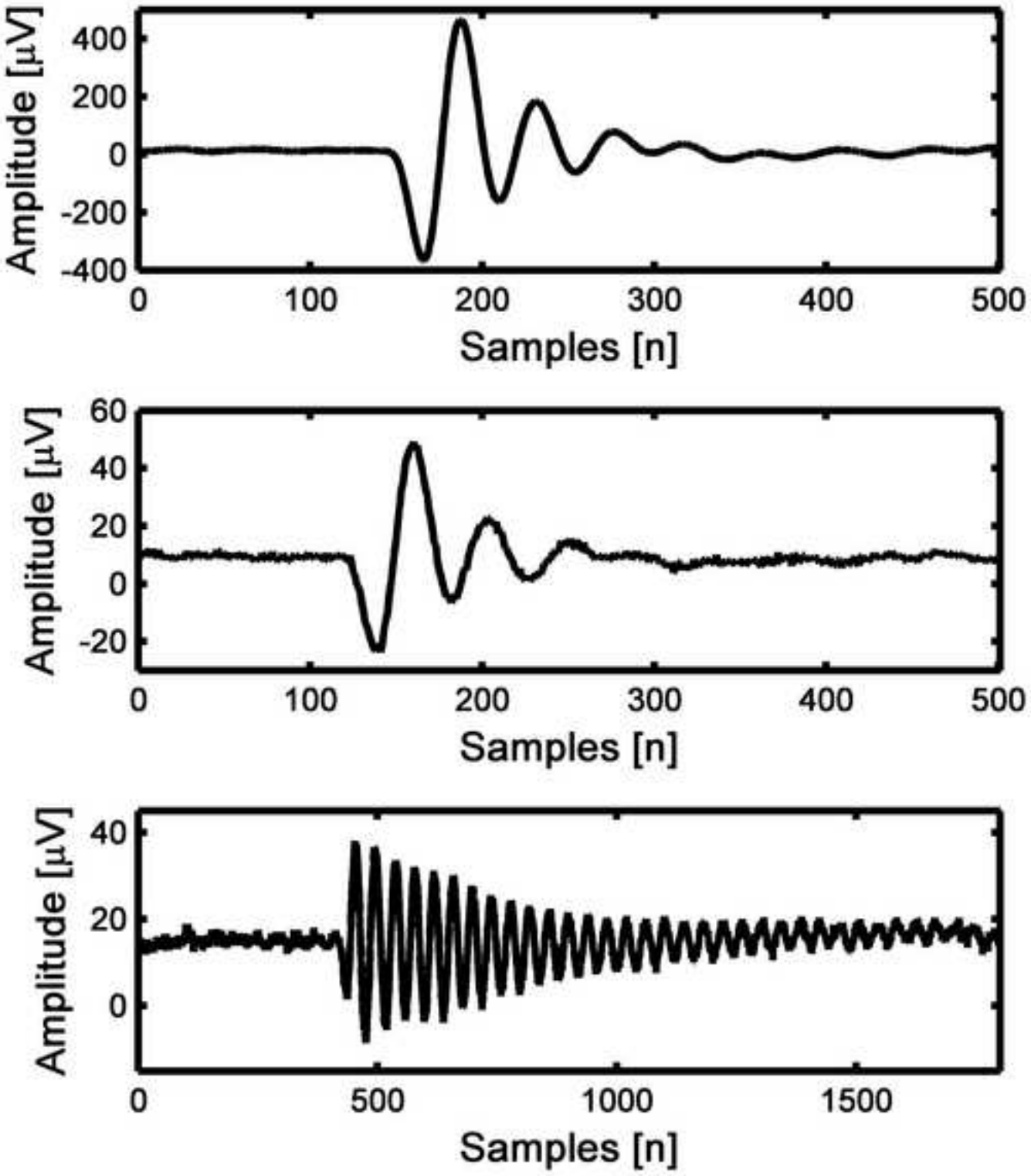

Figure 13
Click here to download high resolution image

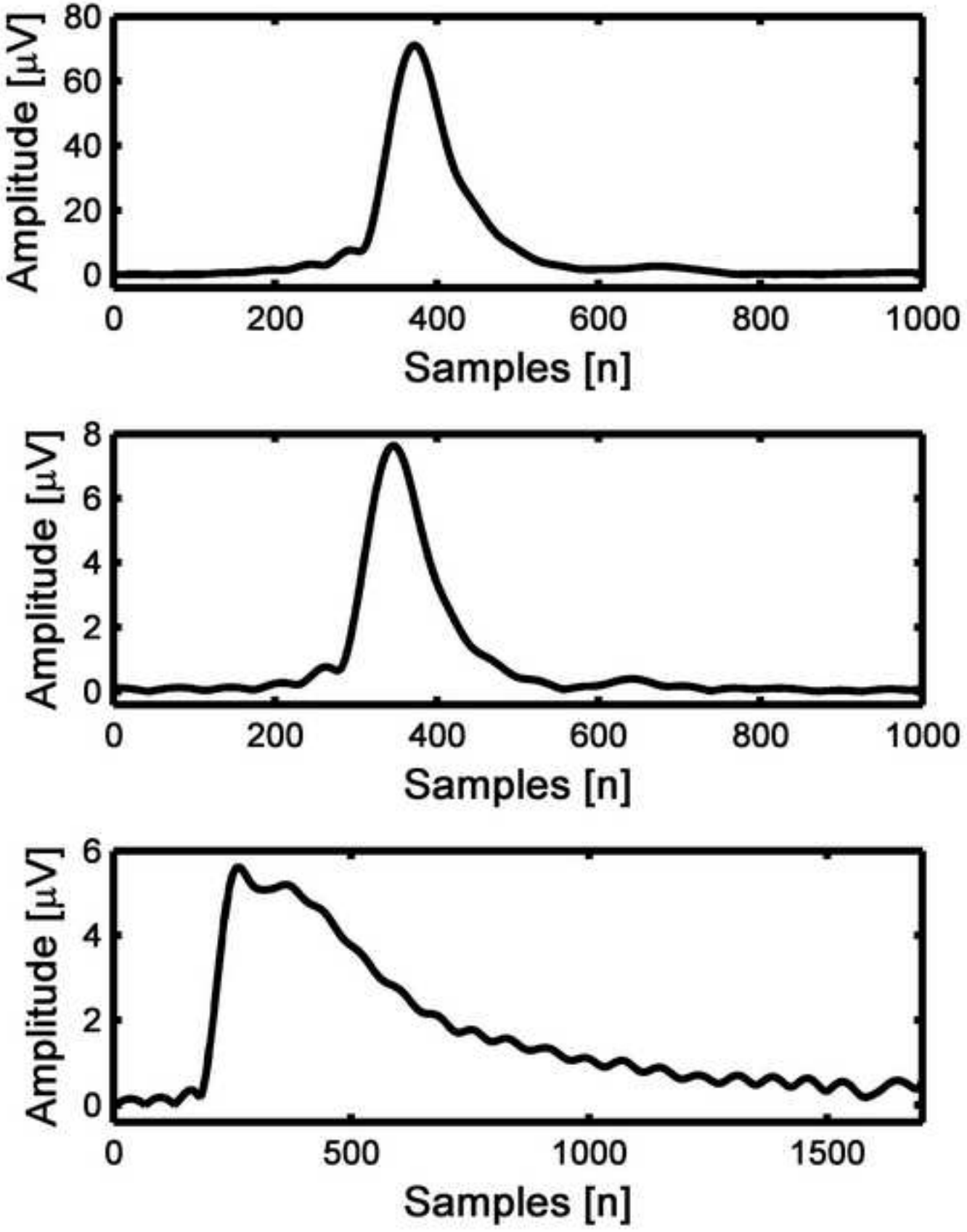

Figure 14
Click here to download high resolution image

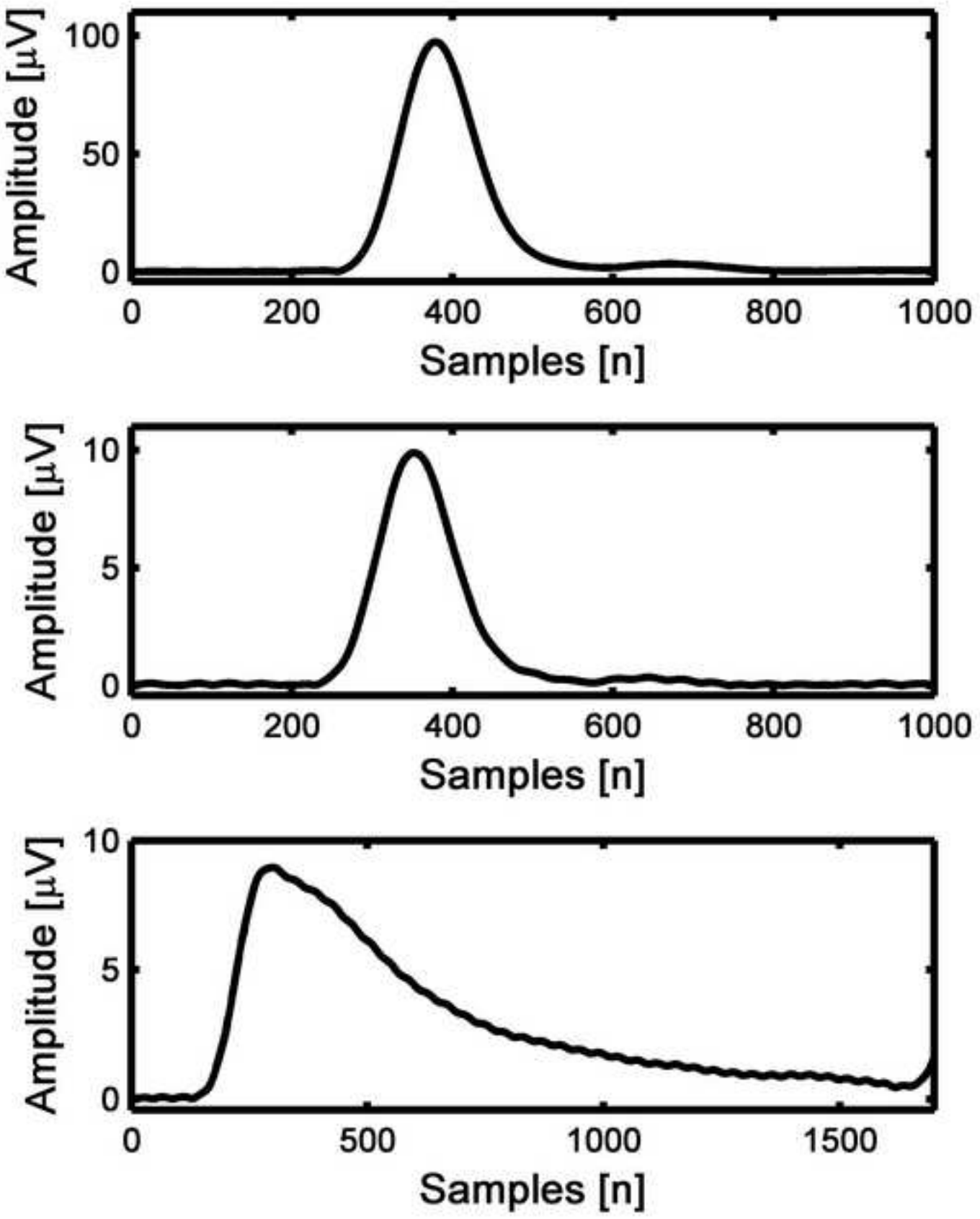

Figure 15

Click here to download high resolution image

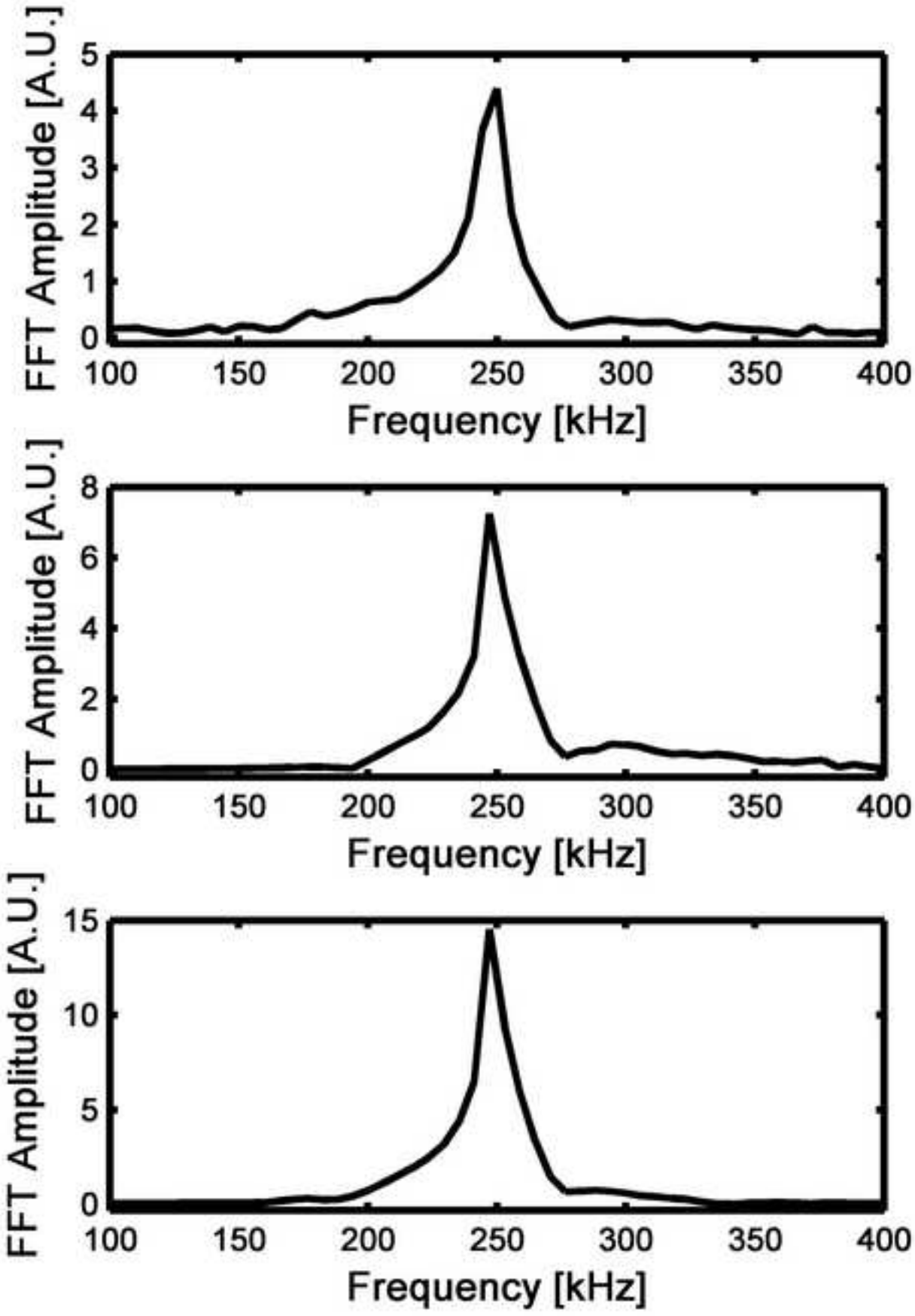

Table 1

Field Region	Type of signal				
	MLS	***Standard linear chirp***	***Cyclic linear chirp***	***Standard non-linear chirp***	***Cyclic non-linear chirp***
Near	97	98	103	104	105
Far	97	112	111	104	105

***Highlights (for review)**

- We demonstrate that pulse compression is a powerful tool for air-coupled ultrasound
- The result is very dependent on the choice of waveform used
- Binary sequences are a good choice where a wide bandwidth is available
- More limited bandwidths are best suited to the use of chirps